IEEE Access
Multidisciplinary ⋮ Rapid Review ⋮ Open Access Journal

Received April 14, 2022, accepted May 1, 2022, date of publication May 3, 2022, date of current version May 9, 2022.

Digital Object Identifier 10.1109/ACCESS.2022.3172418

A Real-Time Maximum Power Points Tracking Strategy Consider Power-to-Average Ratio Limiting for Wave Energy Converter

LIXUN ZHU[1], ZHAOYANG YAO[1], AND WEI LI[2], (Member, IEEE)
[1]Department of Logistics Engineering, Shanghai Maritime University, Shanghai 201306, China
[2]Department of Electrical Engineering, Tongji University, Shanghai 200092, China

Corresponding authors: Lixun Zhu (lixzhu@shmtu.edu.cn) and Wei Li (liweimail@tongji.edu.cn)

This work was supported in part by the National Natural Science Foundation of China under Grant 52007113 and Grant 51777139, in part by the Shanghai Sailing Program under Grant 20YF1416300, and in part by the Shanghai Frontiers Science Center of ''Full Penetration'' Far-Reaching Offshore Ocean Energy and Power.

ABSTRACT Based on the mechanical model of the point absorption Wave Energy Converter (WEC), a real-time complex conjugate (CC) maximum power point tracking (MPPT) control strategy consider power peak-to-average ratio (PAR) limiting under irregular waves is proposed. In the proposed MPPT strategy, the system can not only track the maximum power, but also limit the PAR of the output power to improve the controlled generator's utilization rate. Two parameters, R_{epot} and X_{pto}, that determine the command current of the PMSG and the PAR, are introduced in the mathematical model of the system to control the system. And they are identified by the Grey Wolf Optimization (GWO) algorithm. During each half cycle of the sea wave, the parameters R_{pto} and X_{pto} will be real time updated to satisfy the control strategy. In addition, the system parameters A, B_{rad} and $F(\omega)$ related to wave frequency are also calculated by the advanced quantitative wave analysis (AQWA) software. Finally, the proposed strategy is verified by the comparison on the simulation and the experimental results.

INDEX TERMS Wave energy converter, maximum power point tracking, grey wolf optimization algorithm, permanent magnet synchronous generator.

I. INTRODUCTION

Due to the shortage of traditional fossil energy and its damage to the environment, the development of new energy has attracted the attention of governments all over the world. Among many renewable energy sources, sea wave energy is one of the most potential renewable energy sources, which has the characteristics of high energy density, wide distribution, and good availability [1]–[4]. However, extracting energy from sea waves and converting to electrical energy is quite difficult because of the low-speed linear sea waves motion. At present, based on different design concepts, wave power generation devices suitable for various sea conditions have been developed [5]–[7]. Compared with other wave power generation devices, the point absorption wave energy converter (WEC) consists of a buoy and power take-off (PTO) cylinder is widely researched [8], as shown in Fig. 1, which can fit various sea conditions, absorb incident waves in various directions, and have high wave energy capture efficiency [9].

Improving the power captured by WEC has always been a research hotspot in the field of wave power generation. For WEC, in addition to energy capture mechanism and device design and development, it is important to introduce control to enlarge the energy absorption and broaden the bandwidth. Already during the mid-1970s it was proposed independently by Salter and Budal to apply control engineering for optimizing the oscillatory motion of a WEC in order to maximize the energy output. Research shows that by changing the control force exerted on the buoy, the inherent properties of WEC can be changed, so that the WEC can resonate with the waves to increase the power captured by the WEC [10].

Based on the resonance concept, several control strategies are proposed by researchers, mainly including: 1) Latching control: The latching control is a discrete nonlinear phase control scheme, which was first proposed by Budal and

The associate editor coordinating the review of this manuscript and approving it for publication was Chi-Seng Lam.

Falnes [11]–[13]. They found that one condition for maximizing energy absorption was to keep the velocity in phase with the wave excitation force, thus requiring an additional device to lock the buoy. However, the applicability of the latching control method has been questioned because an additional mechanism needs to be configured to hold the buoy, and the control response may be slow due to the mechanical configuration [14], [15]. 2) Passive loading (PL) control: This method controls the amplitude of the movement by modifying the dynamic damping of the PTO, which requires a force provided by the PTO that is proportional to the speed of the buoy; Since the energy flows in one direction, the energy captured by this control method is small. 3) Complex conjugate (CC) control: This method requires controlling of the generator to keep the system in resonance, requiring extensive power exchange between the oscillating system and the PTO system. However, the power peak-to-average ratio (PAR) is too high, so that the system performance is low [5], [6]. To implement the above control strategies, the mathematical modeling with its parameters should be developed. The parameters of the system modeling are non-linear and are function of the sea conditions and the buoy status. Therefore, accurate identification of the system paraments is not easy. Based on the above, some research contents have been published. For example, a hill-climbing-based maximum power point tracking (MPPT) control strategy is proposed in [16]. In [13], a piecewise velocity control method based on latching control is proposed. For the simplicity of the analysis, the WEC model parameters adopt in [13] and [16] are fixed values, while the actual WEC parameters change with the excitation force, which may affect the accuracy of the analysis results.

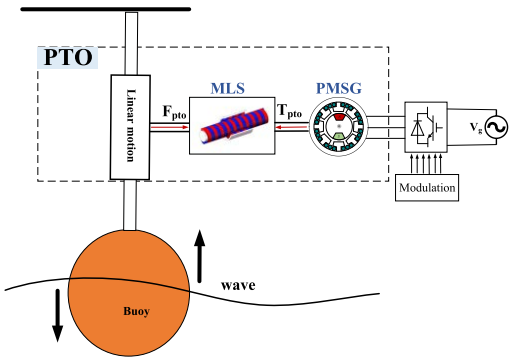

FIGURE 1. Point absorption wave power generation device.

In this paper, under the irregular wave conditions, a real-time CC MPPT control strategy considering power PAR limiting is proposed. In the proposed MPPT strategy, the system can not only track the maximum power, but also limit the PAR of the output power to improve the controlled generator's utilization rate. Two parameters, R_{pto} and X_{pto}, that determine the command current of the PMSG and the PAR, are introduced in the mathematical model of the system to control the system. And they are identified by. During each half cycle of the sea wave, the parameters R_{pto} and X_{pto} will be real time updated by the Grey Wolf Optimization (GWO) algorithm to satisfy the control strategy. In addition, the system parameters A, B_{rad} and $F(\omega)$ related to wave frequency are also calculated by the advanced quantitative wave analysis (AQWA) software. Finally, the proposed strategy is verified by the experimental results.

This paper is organized as follows. In Section II, the wave surface displacement of a specific sea state and the exciting force acting on the buoy will be obtained. The hydrodynamic model and equivalent *RLC* circuit model of WEC are analyzed. In Section III, the traditional control methods and the conditions for capturing the maximum energy are introduced. The effect of PAR in the control process is introduced. In Section IV, a GWO-based real-time CC MPPT control strategy considering power PAR limiting under irregular waves is proposed. And introduced its control process and flow chart. In Section V, Simulations under regular wave and irregular wave conditions are performed to evaluate the capability of the proposed control method. In addition, the results using the traditional control methods are compared. Experiments verify the effectiveness of the proposed control method. And the applicability is experimentally verified. Finally, some conclusions are discussed in Section VI.

II. THE EQUIVALENT MODELING OF WEC BASED ON POINT ABSORPTION

A. IRREGULAR WAVES AND EXCITING FORCE

The excitation force of the buoy drives the operation of the WEC system, and the excitation force is usually irregular because of the complex sea condition [17]. The modeling of the excitation force is necessary.

A linear long-crested irregular wave motion under an arbitrary sea condition can be expressed by the superposition of a series sinusoidal waves whose amplitudes, frequencies, and phases are different in the linear sea wave theory as

$$\eta(t) = \sum_{n=1}^{M} \eta_n(t) = \sum_{n=1}^{M} A_n \cos(\omega_n t + \varepsilon_n) \tag{1}$$

where η is the height of the irregular wave, M is the number of sinusoidal waves. A_{n}, ω_n and ε_{n} are the amplitude, angular velocity and phase corresponding to the n-th regular waves, respectively. A_{n} can be obtained from the Rayleigh distribution as

$$E\left[A_n^2\right] = 2S(\omega_n)\Delta\omega \tag{2}$$

where S is the wave spectrum, and $\Delta\omega$ is the frequency interval of each component wave. $\Delta\omega$ is determined by the duration of the irregular wave, $\Delta\omega = 2\pi/T_{\mathrm{total}}$, and T_{total} is the total duration of a modeling irregular wave. S can be defined from several well-defined wave power spectra, such as Pierson-Moskowitz (PM), Breitscheider and JONSWAP spectrum, which are commonly encountered in the marine engineering literature [18], [19]. In this paper,

$S(\omega_n)$ is defined from the Bretschneider spectrum [20], as follows

$$\begin{cases} S(\omega_n) = \dfrac{5}{16} H_{1/3}^2 \dfrac{\omega_m^4}{\omega_n^5} e^{-\frac{5}{4}\left(\frac{\omega_m}{\omega_n}\right)^4} \\ \omega_m = \dfrac{2\pi}{T_m} \end{cases} \tag{3}$$

where ω is frequency of the wave, ω_m is the modal (most likely) frequency of any given sea state, and $H_{1/3}$ is the significant wave height. In the Bretschneider spectrum, the ω_m and $H_{1/3}$ under any sea state can be obtained from Table 1.

Then the excitation force applied on the buoy can be calculated as follows [21]

$$F_{exc}(t) = \sum_{n=1}^{M} \eta_n(t) F(\omega_n) \tag{4}$$

where $F(\omega_n)$ is the excitation force corresponding to the unit amplitude of frequency ω_n, which is obtained by AQWA software simulation.

TABLE 1. Information in different sea conditions.

Sea State	$2\pi/\omega_m$, sec	$H_{1/3}$
2	6.3	0.3 m
3	7.5	0.9 m
4	8.8	1.9 m
5	9.7	3.3 m
6	12.4	5.0 m

B. EQUIVALENT MODELING OF WEC

For the point absorber type WEC, as shown in Fig. 1, it mainly consists of two parts: buoy and PTO. The buoy can only move in one degree of freedom, that is, it moves vertically by the sea waves. The linear motion of the buoy with the ups and downs of the wave is converted into rotational motion by the magnetic lead screw (MLS) [4], which drives the rotational generator.

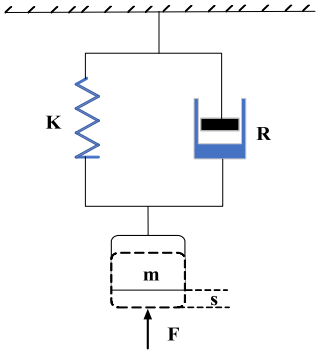

FIGURE 2. Spring-block system.

The WEC system as shown in Fig. 1 can be surmised by the basic spring-block system, as shown in Fig. 2. In Fig. 2, K is the elastic coefficient of the spring, R is the coefficient of the damping, m is the mass of the block, and $\boldsymbol{s}$ is the displacement of the block which is driven by the external force $\boldsymbol{F}$. According to the Newton's second law, the system of the WEC in Fig.1 can be modeled as following [22], [23]

$$(M + A(\omega))\ddot{s}(t) + (B_{rad}(\omega) + k_{c1})\dot{s}(t) + K_s s(t) = F_{exc}(t) - F_{pto}(t) \tag{5}$$

where ω is the angular frequency of the incident wave, M is the mass at rest of the device, $\boldsymbol{s}$ is the position of the buoy. A is the added mass considering the frequency of the incident wave, B_{rad} is the radiation damping coefficient at the considered frequency. Among them, A and B_{rad} are also determined by the shape of the buoy, and they can be identified from the hydrodynamics. In this paper, The WEC system is simulated by the AQWA software simulation, then the parameters can be obtained. K_s is the hydrodynamic stiffness, and $K_s = \pi\rho g r^2$, r is the radius of the buoy, ρ is the density of sea water, and g is the gravitational acceleration. k_{c1} is the friction coefficient of the WEC. F_{exc} is the exciting force of the wave acting on the system, as shown in (4). F_{pto} represents the external controllable force acting on the system by PMSM through MLS transformation.

The control idea of WEC is to compensate the buoy by controlling the output torque T_{pto} of the PMSM, so that the velocity of the buoy and the exciting force are in phase as much as possible. In the proposed WEC in this paper, the F_{pto} in (6) is transferred from the T_{pto} by MLS as [24]

$$F_{pto}(t) = k \cdot T_{pto}(t) \tag{6}$$

where k is the transmission ratio of the MLS. Also, the mechanical angular velocity of the PMSM Ω_m can be expressed as

$$\Omega_m(t) = k \cdot \dot{s}(t) \tag{7}$$

And the PMSM can be modeled under d-q axis by

$$\begin{cases} T_{pto} - T_e = J\dfrac{d\Omega_m}{dt} + B_s\Omega_m \\ T_e = \dfrac{3}{2} p_n \lambda_{dr} i_{qs} \end{cases} \tag{8}$$

where T_e is the electromagnetic torque, J is the moment of inertia of the PMSM, B_s is the viscous friction coefficient, P_n is the number of pole pairs of the PMSM, λ_{dr} is the rotor d-axis magnetic flux, and i_{qs} is the stator q-axis current. In this paper, the vector control method of PMSM under the stator d-axis current $i_{ds} = 0$ condition is adopted to control T_e, and command current i_{qs} can be expressed as

$$i_{qs} = \frac{2F_{pto}}{3kp_n\lambda_{dr}} - \frac{2k(J\ddot{s}(t) + B_s\dot{s}(t))}{3n_p\lambda_{dr}} \tag{9}$$

For simplicity of analysis, (5) can be equivalent to an *RLC* analog circuit when consider the $\dot{s}(t)$ to the current in the circuit theory [25], as shown in Fig. 3.

Then, the exciting force $F_{exc}(t)$ is represented by the voltage source $E(t)$, R_{pto} and X_{pto} represents the impedance

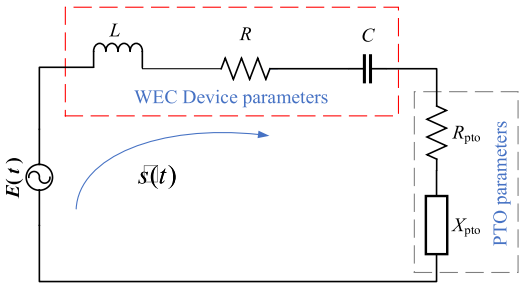

FIGURE 3. Analog RLC circuit of a point absorber WEC.

of F_{pto}. Though (5), (6), (7) and (8), the parameters of R, L, C in Fig. 3 can be expressed

$$\begin{cases} L = M + A(\omega) + k^2 J \\ R = B_{rad}(\omega) + k_{c1} + k^2 B_s \\ C = \dfrac{1}{K_s} \end{cases} \tag{10}$$

III. TRADITIONAL MPPT CONTROL METHOD

A. PL CONTROL

In the PL control method, $X_{pto} = 0$ in Fig. 3. To obtain the maximum possible extraction of average power under such condition, the resistive component in the Fig. 3 can be obtained as

$$R_{pto} = \sqrt{R^2 + (\omega L - \frac{1}{\omega C})^2} \tag{11}$$

The maximum average power extracted can be calculated

$$\bar{P}_{pl} = \frac{E^2 \cdot R_{pto}}{(R + R_{pto})^2 + (\omega L - \frac{1}{\omega C})^2} \tag{12}$$

Therefore, in order to capture the maximum power, F_{pto} can be obtained as

$$F_{pto} = R_{pto}\dot{s}(t) \tag{13}$$

B. CC CONTROL

In the CC control, in order to extract the maximum power, the parameters X_{pto} and Rpto in Fig. 3 can be obtained as

$$\begin{cases} \omega L - \dfrac{1}{\omega C} - X_{pto} = 0 \\ R = R_{pto} \end{cases} \tag{14}$$

And the maximum power absorbed by the load can be obtained as follows

$$\bar{P}_{cc} = \frac{E^2 \cdot R_{pto}}{(R + R_{pto})^2 + (\omega L - \frac{1}{\omega C} - X_{pto})^2} \tag{15}$$

Also, F_{pto} can be obtained as

$$F_{pto} = R_{pto}\dot{s}(t) + \frac{X_{pto}}{\omega}\ddot{s}(t) \tag{16}$$

C. PEAK-TO-AVERAGE RATIO

Peak-to-average ratio k_{PAR} is an important parameter to evaluate the performance of the WEC output power, and it is defined as

$$\begin{cases} k_{PAR} = \dfrac{\hat{P}}{\bar{P}} = 1 + \dfrac{1}{\cos\varphi_{pto}} \\ \varphi_{pto} = \arctan(\dfrac{X_{pto}}{R_{pto}}) \end{cases} \tag{17}$$

where X_{pto}, R_{pto} are the inductance and resistance of the load in Fig. 3, and the property of the k_{PAR} is illustrated in Fig. 4. It can be seen from (17) that under the same wave, smaller k_{PAR} means better quality of the extracted energy and higher utilization rate of the PMSM. However, the average power captured is limited if the value of k_{PAR} is quite small.

In PL control method, the k_{PAR} is fixed at 2 because of $X_{pto} = 0$. Though the k_{PAR} is the lowest in Fig. 4, the maximum extracted average power $\bar{P}_{\mathrm{pl}}$ is not satisfied after compared with the $\bar{P}_{\mathrm{cc}}$ in (15).

The maximum extracted average power $\bar{P}_{\mathrm{cc}}$ is higher in CC control, however, the k_{PAR} is also quite high [26]. It means if the CC control method is adopted to tracking the maximum power, the utilization rate of the PMSG is very low.

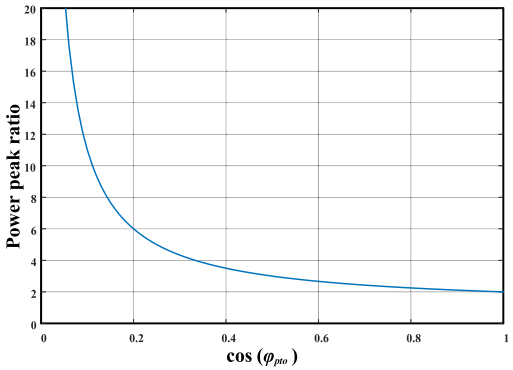

FIGURE 4. Power peak-to-average ratio under different PTO loads.

IV. PROPOSED REAL-TIME MPPT CONTROL STRATEGY

A. THE MPPT CONTROL METHOD

To not only consider the utilization rate of PMSM, but also improve the maximum extracted average power, a GWO-based real-time CC MPPT control strategy considering power PAR limiting under irregular waves is proposed in this paper. The process of the control strategy is as:

Step 1: Obtain a half cycle sea wave η by using the zero-crossing frequency detection method.

Step 2: Calculate the corresponding F_{exc} by using (4).

Step 3: Calculate the frequency of the half cycle sea wave and obtain the hydrodynamic parameters by using linear interpolation method.

Step 4: Determine the R_{pto} and X_{pto} by GWO algorithm under the following condition

$$k_{\mathrm{PAR}} \leq k_{\max} \tag{18}$$

to obtain the maximum value $\bar{P}_{cc}$ in (15), and k_{max} is depend on the sea state and the rated parameters of the PMSM. It is identified from the trial and error method when the rotational speed (Rev) and Torque is closed to the rated value.

Step 5: Apply the obtained optimum value R_{pto} and X_{pto} to the system in the next half cycle sea wave.

B. IMPLEMENT WITH GWO ALGORITHM

The GWO algorithm is a population-based meta-heuristic algorithm, which simulates the mechanism of gray wolf group collaboration in the biosphere to achieve the purpose of optimization [27]. The optimal solution in the wolf pack is α, which is the X_{pto} and R_{pto}. The β, δ are the second and third best solutions, respectively, representing the sub-solution set of X_{pto} and R_{pto}. The remaining candidate solutions are χ, representing the candidate set of the optimal solution. In the GWO algorithm, the hunting (optimization) is guided by α, β and δ wolves together, and the χ wolf follows these three wolves to update the position. The mathematical model of the hunting behavior of gray wolves is as follows

$$\begin{aligned} \boldsymbol{D} &= \left|\boldsymbol{C} \cdot \boldsymbol{X}_p(t) - \boldsymbol{X}(t)\right| \\ \boldsymbol{X}(t+1) &= \boldsymbol{X}_p(t) - A \cdot D \end{aligned} \tag{19}$$

where $\boldsymbol{D}$ represents the distance between the prey and the individual gray wolf, $\boldsymbol{X}$ is used to update the position of the gray wolf, $\boldsymbol{X}_p$ is the prey position vector, $\boldsymbol{X}$ is the gray wolf position vector. $\boldsymbol{A}$ and $\boldsymbol{C}$ are coefficient vectors, the calculation formula is as follows

$$\begin{aligned} \boldsymbol{A} &= 2a \cdot \boldsymbol{r}_1 - a \\ \boldsymbol{C} &= 2\boldsymbol{r}_2 \end{aligned} \tag{20}$$

where a is the convergence factor that linearly decreases from 2 to 0 as the number of iterations. $\boldsymbol{r}_1$ and $\boldsymbol{r}_2$ represent random numbers between 0-1. The position of the ω wolf in the population is jointly determined by the positions of α, β and δ:

$$\begin{cases} \boldsymbol{D}^j_{i,\alpha}(t) = \left|\boldsymbol{C}_1 \cdot X^j_\alpha - \boldsymbol{X}_i(t)\right| \\ \boldsymbol{D}^j_{i,\beta}(t) = \left|\boldsymbol{C}_1 \cdot X^j_\beta - \boldsymbol{X}_i(t)\right| \\ \boldsymbol{D}^j_{i,\delta}(t) = \left|\boldsymbol{C}_1 \cdot X^j_\delta - \boldsymbol{X}_i(t)\right| \end{cases} \tag{21}$$

$$\begin{cases} \boldsymbol{X}_{i,\alpha}(t) = \boldsymbol{X}^j_\alpha - \boldsymbol{A} \cdot \boldsymbol{D}^j_{i,\alpha}(t) \\ \boldsymbol{X}_{i,\beta}(t) = \boldsymbol{X}^j_\beta - \boldsymbol{A} \cdot \boldsymbol{D}^j_{i,\beta}(t) \\ \boldsymbol{X}_{i,\delta}(t) = \boldsymbol{X}^j_\delta - \boldsymbol{A} \cdot \boldsymbol{D}^j_{i,\delta}(t) \end{cases} \tag{22}$$

$$\boldsymbol{X}^j_i(t+1) = \frac{\boldsymbol{X}^j_{i,\alpha}(t) + \boldsymbol{X}^j_{i,\beta}(t) + \boldsymbol{X}^j_{i,\delta}(t)}{3} \tag{23}$$

In (21), $\boldsymbol{D}_i$ represents the distance between the current gray wolf individual and the respective α, β, and δ individuals. The (22) defines the distance that χ wolf moves to α, β, and δ respectively. The (23) defines the final position of χ.

The flowchart of calculating X_{pto} and R_{pto} using the GWO algorithm is shown in Fig. 6. The WEC power tracking control process is shown in Fig. 5.

V. SIMULATION AND EXPERIMENTAL RESULTS

In this paper, the proposed control strategy is applied and varied to the modeled WEC system in Simulink environment of MATLAB software. The specification of the buoy in the modeled WEC system is shown in Table 2.

Also, an experimental test was performed to verify the applicability of the proposed strategy using a dynamometer system as shown in Fig. 5. The test bed was designed for a rated buoy speed of 4.13 m/s, corresponding to a 1,500 rpm dynamo generator speed. In the system, the item of the

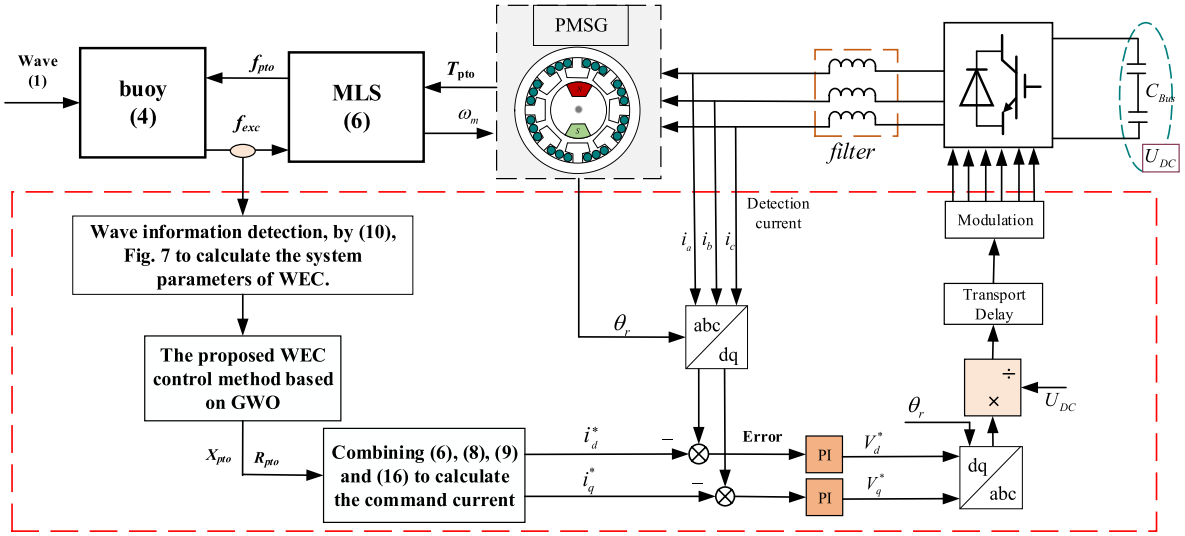

FIGURE 5. GWO-based WEC control diagram.

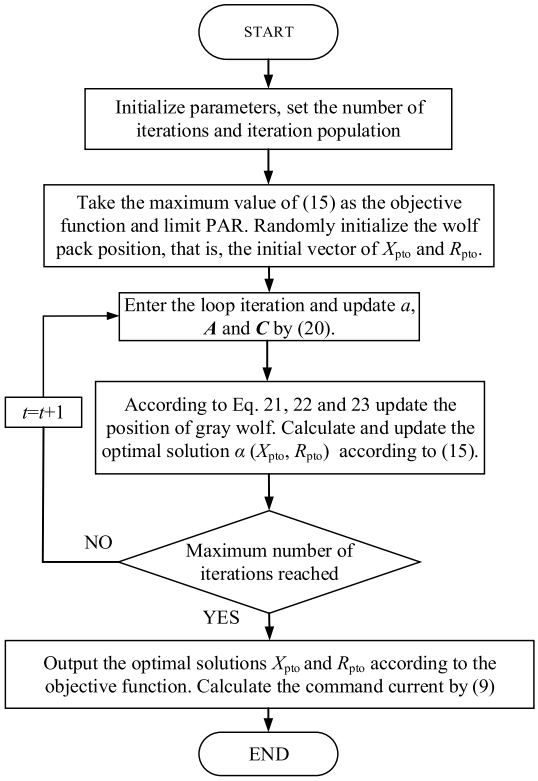

FIGURE 6. Flowchart of the GWO-based control of the WEC system.

PMSM and PMSG are same, and their specification are listed in Table 3.

A. HYDRODYNAMIC SIMULATION RESULTS

To test the performance of the proposed control technique, the $F(\omega)$ of the buoy and the hydrodynamic parameters A, B_{rad} in (5) are calculated by AQWA software, the results are as shown in Fig. 7(a), (b) and (c).

Then the F_{exc} applied on the buoy under the sea state 5 can be calculated by using (4), and the results are shown in Fig. 8(c). The target spectrum under sea state 5 are shown in Fig. 8(a), where the parameter of the target spectrum are

TABLE 2. The parameters of buoy in static.

Symbol	Meaning	Value
r	Buoy radius	5 m
M	Buoy mass	261800 Kg
S	Sea state	5
H_D	Draft	2.5 m
L_D	Drainage volume	130900 Kg
O	Center of gravity, vertical/horizontal/vertical	0 m
I	Moment of Inertia around xyz axis	2619124 Kg • m^2

TABLE 3. The parameters of synchronous test bench.

Symbol	Meaning	Value
P_n	Pole number	4
n_{rate}	Rated Rev	1500 rpm
T_{rate}	Rate torque	15 N*m
K_e	Torque constant	1.13 N*m/A
L_d	d-axis inductance	1.71 mH
L_q	q-axis inductance	1.41 mH
f_s	Switching frequency	10 kHz
k	Gear ratio of MLS	38
U_{dc}	DC voltage	580 V

$\omega_m = 0.65$, $H_{1/3} = 3.3$ m, and the generated irregular wave, which will apply on the buoy, is shown in Fig. 8(b).

Due to the amplified of the simulated F_{exc}, A, B_{rad} and K_s under sea state 5 is too large to develop the experimental test, it is scaled by $1.8*10^{-4}$ in the MPPT control simulation and its experimental test.

B. MPPT CONTROL SIMULATION RESULTS

The detected frequency result of every half period wave in Fig. 8(b) is shown in Fig. 10(a). The parameters R and L under every half period are calculated and shown in Fig. 10 (b) and (c). The capacitance value C in Fig. 3 is 7.08×10^{-3} according to (10).

In this simulation model, the limiting PAR k_{max} is 7.16 under the sea state 5. And the optimum X_{pto} and R_{pto} under the exciting wave in 1500s shown in Fig. 9.

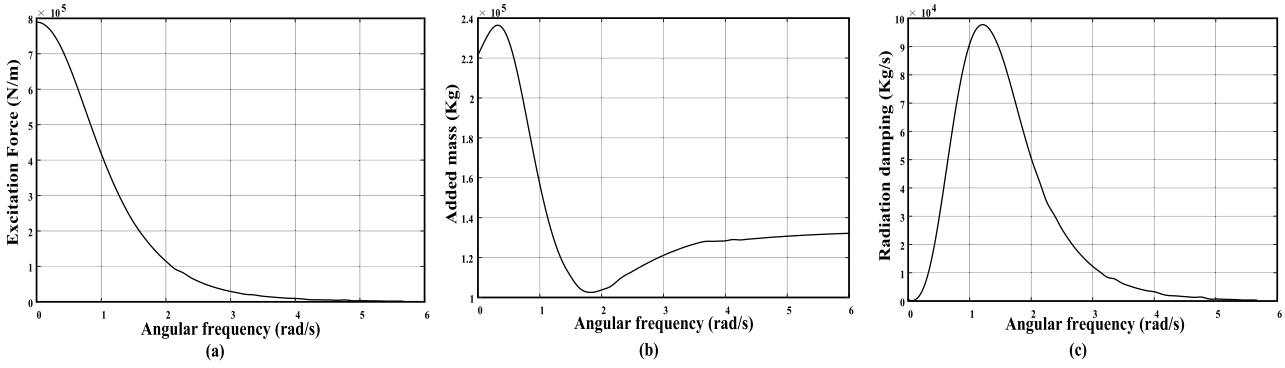

FIGURE 7. ANSYS AQWA numerical analysis results. (a) Exciting force per unit wave amplitude. (b) Added mass. (c) Radiation dapming value.

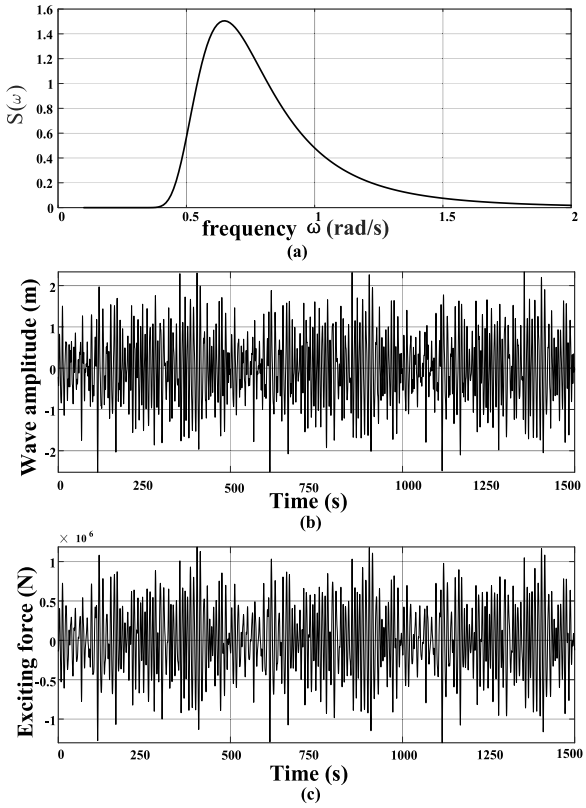

FIGURE 8. Results of irregular wave generation: (a) Bretschneider spectrum. (b) wave amplitude. (c) exciting force.

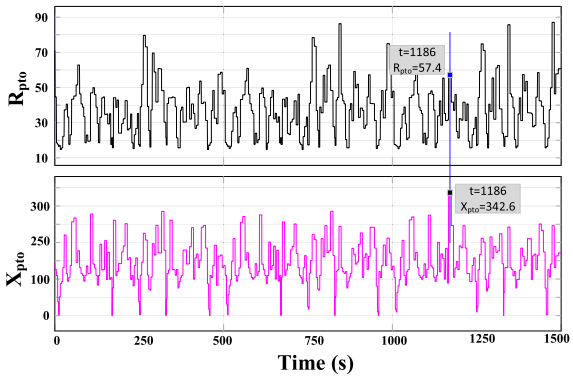

FIGURE 9. X_{pto}, R_{pto} calculated based on GWO.

Since the hydrostatic coefficient K_s of the buoy is greater than the buoy mass and the additional mass, the WEC system is always in a capacitive state, combined with (10) and (14), it can be observed from Fig. 9 that the X_{pto} calculated based on the complex conjugate control of GWO always positive. When t = 1186s, $X_{pto} = 342.6$ and $R_{pto} = 57.4$, there is the largest PAR, which is 7.05, and is less than $k_{\max} = 7.16$.

Under irregular waves, using the proposed control method, the simulation results of the absolved excitation force and the speed of the buoy are shown in Fig. 11. It can be seen from the Fig. 11 that the speed and the exciting force are almost

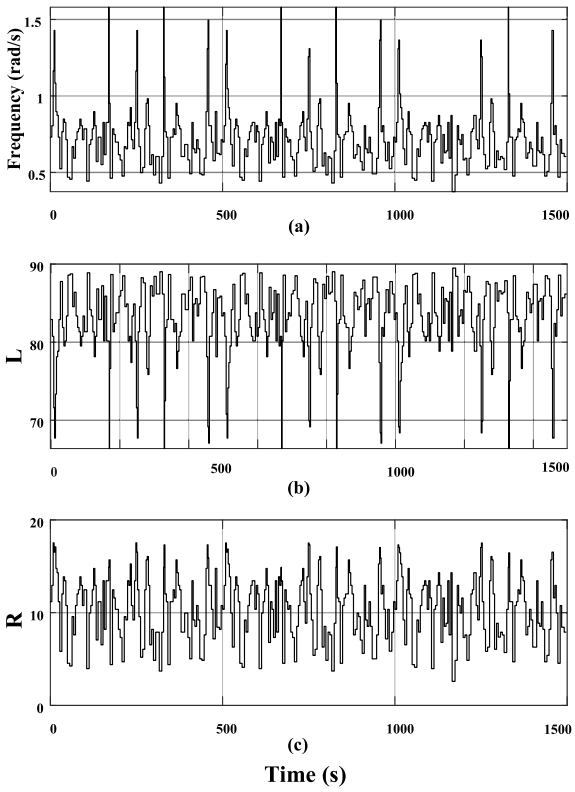

FIGURE 10. Frequency of the exciting force and analog circuit parameters R(ω), L(ω).

in phase, which indicates that the WEC system is in a state of resonance, and the energy captured by the system from the waves is at a maximum.

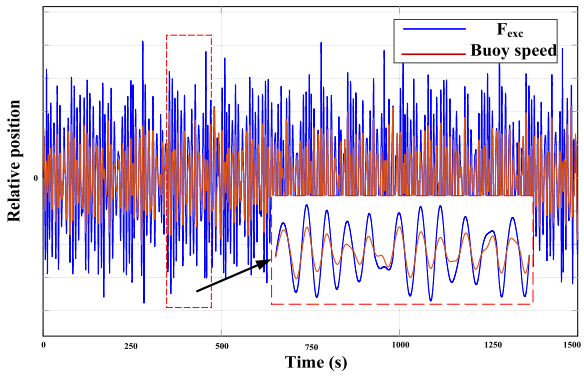

FIGURE 11. The excitation force and buoy speed.

In order to verify the advantages of the proposed control method with respect to traditional PL and CC control when applied in irregular waves, their simulation results must be compared and analyzed. Under the same irregular wave, as shown in Fig. 8(b), the simulation results of different control methods are shown in Fig. 12, and more comparison results are presented in Table 4. Accordingly, to the

previously presented control analysis, it is here assumed that the considered system is equipped with a PMSG as shown in Table 3, whose rated Rev is 1500 rmp, and rated torque is 15 N*m.

Using the proposed control method, the simulation results are shown in Fig. 12(a). It can be seen from Fig. 12(a), the torque and Rev of the PMSG within 1500 s are presented, and the average power extraction, calculated as the average of the instantaneous power along the entire 1500 s simulation, is $P_{avg} = 84.16$ W, and the peak power is $P_{max} = 1013.58$ W. In this case, the rms value of the torque and Rev are $T_{rms} = 5.9$ N*m and $n_{rms} = 577$ rpm respectively [Table 4], both below the rated value of the PMSG. The peak value of the torque and Rev are $T_{max} = 14.5$ N*m and $n_{max} = 1486$ rpm respectively [Table 4], also below the limit of PMSG rated value.

TABLE 4. Simulation results of the propose method, CC and PL method.

	P_{avg} (W)	T_{rms} (N*m)	n_{rms} (rpm)	T_{max} (N*m)	n_{max} (rpm)	PAR_{max}
Proposed control	84.16	5.9	577	14.5	1486	7.05
CC control	109.69	15.6	1360	46.1	4126	74.63
PL control	23.08	1.5	157	4.9	544	2

If the CC control method is applied and other conditions remain the same, the simulation results are shown in Fig. 12(b). As can be seen from Fig. 12(b), the average power is $P_{avg} = 109.69$ W and the peak power is $P_{max} = 8124.56$ W. Compared to the proposed method, although its average power extraction is improved by 29.7%, the CC control would be completely unsustainable. Because in this case, the peak value of the torque and Rev are $T_{max} = 46.1$ N*m and $n_{max} = 4126$ rpm respectively [Table 4], which is far beyond the PMSG's rated value, causing it to not operate normally. Not only that, it can be noticed that the PAR of the CC control method is $k_{max} = 74.63$ much larger than the $k_{max} = 7.05$ of the proposed method. Fig. 12(c) shows the results of the PL control method being applied, the average power is $P_{avg} = 23.08$ W and the peak power is $P_{max} = 196.72$ W. In this case, $T_{rms} = 1.5$ N*m, $n_{rms} = 157$ rpm, $T_{max} = 4.9$ N*m and $n_{max} = 544$ rpm [Table 4], all of which are far smaller than the PMSG's rated value, which leads to the underutilized PMSG's capacity. Although $k_{PAR} = 2$, its average power is $P_{avg} = 23.08$ W, which is only 27.4% of the proposed method.

Finally, by comparing the PL and CC control methods, under the condition of irregular waves, it is proved that the proposed method can fully utilize the capacity of the PMSG and achieve the purpose of emitting the maximum average power.

C. EXPERIMENTAL RESULTS

In the experiment, the calculated buoy speed was converted to the PMSM speed and used as the speed command in the dynamo motor drive. The control block diagram and experimental equipment are shown in Fig. 13 and 14.

Fig. 15 shows that the experimental results of the excitation force and the Rev of PMSG from 200 to 500 seconds, due to the limitations of the oscilloscope. It can be seen that the phases of the excitation force and the PMSG speed are basically same. Meanwhile, the maximum Rev of PSMG is less than the rated value, which meets the requirements of equipment operation. This shows that using the proposed method, the WEC system can resonate with waves, increasing the power captured by the WEC system.

The simulated and experimental values of PMSG speed and torque are shown in Fig. 16(a) and (b). It can be seen from the Fig. 16 that the experimental Rev and torque are in good agreement with the simulation results. It shows that the proposed control method performs well in the control of the PMSG, which proves the feasibility of the method in the practical sense.

Finally, the Fig. 17 shows the instantaneous power and average power range from 200s to 800s. It can be seen

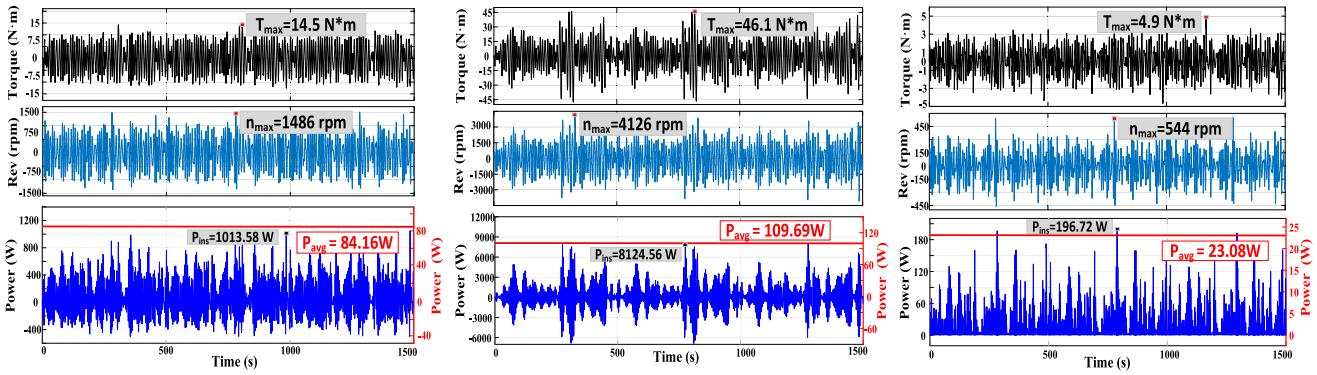

(a) (b) (c)

FIGURE 12. (Top) torque and Rev of PMSG and (bottom) instantaneous and average power in the cases of (a) proposed control, (b) CC control, and (c) PL control. The rated torque and Rev of PMSG are 15 N*m and 1500 rpm.

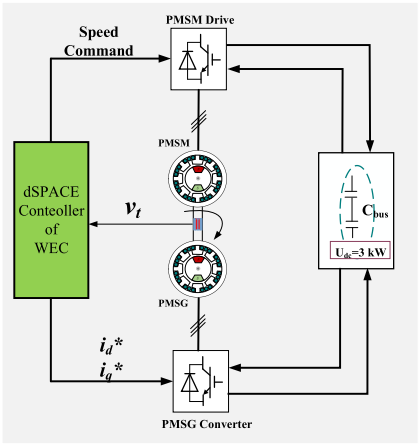

FIGURE 13. Control block diagram.

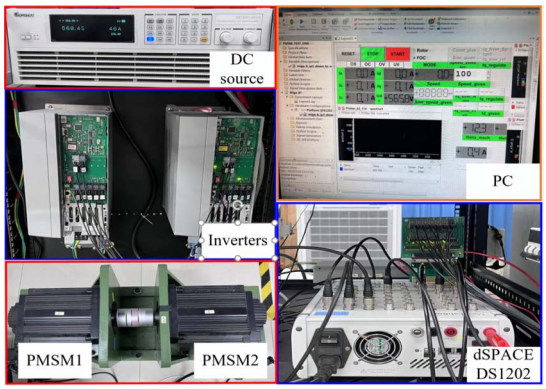

FIGURE 14. Experimental test bench.

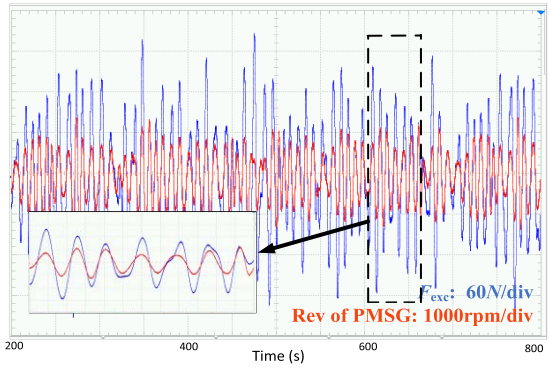

FIGURE 15. Experimental results of excitation force and PMSG speed.

from the Fig. 17 that the average power of the experiment is approximately close to the theoretical value of 84.16 W, which is due to the existence of friction and other reasons that make the actual value smaller than the theoretical value.

The experimental results presented above demonstrate that the proposed method has successfully achieved MPPT operation with irregular waves. Additionally, the proposed

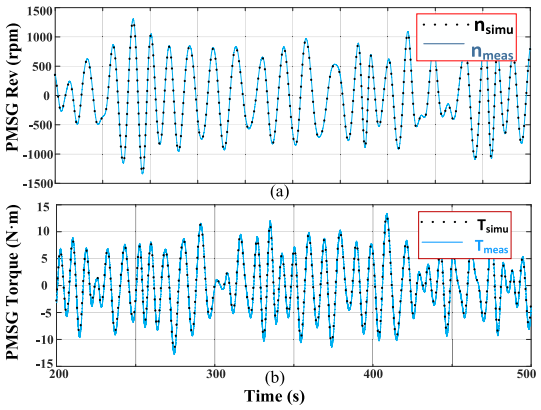

FIGURE 16. Experimental result: (a) the simulated and measured Rev of the PMSG, (b) the simulated and measured torque of PMSG.

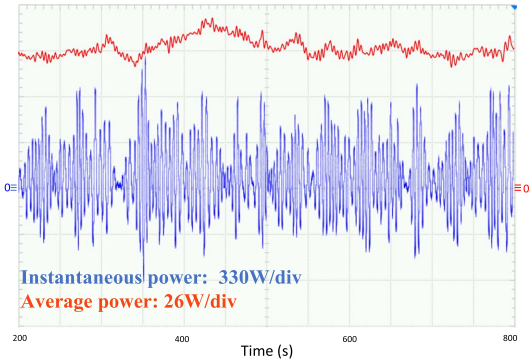

FIGURE 17. Experimental results of instantaneous power and average power.

technique enables to consider simultaneously both the torque and Rev of PMSG and the PAR limit, which is significant for a WEC system in order to operate safely and efficiently.

VI. CONCLUSION

In this paper, under the irregular wave conditions, a GWO-based real-time CC MPPT control strategy considering power PAR limiting under irregular waves is proposed. The irregular wave (η) and the corresponding excitation force under specific sea condition are calculated. The WEC system parameters A, B_{rad} and $F(\omega)$ related to wave frequency (ω) are calculated by AQWA software and the equivalent circuit model and mathematical expression are analyzed.

The parameters R_{pto} and X_{pto} that determine PAR at each half cycle are calculated by the GWO algorithm. With parameters R_{pto} and X_{pto} at each half cycle, the command current to control the PMSG is calculated. The performance of PL control, CC control and the proposed control method under irregular waves is compared, and the simulation results demonstrate the superiority of the proposed control method. The simulation and experimental results show that the proposed control method can not only emit a larger average power, but also a higher utilization rate of PMSG, which proves the effectiveness of this method.

REFERENCES

[1] S. O. Pinto, P. R. Santos, and F. T. Pinto, "Assessment of the potential of combining wave and solar energy resources to power supply worldwide offshore oil and gas platforms," *Energy Convers. Manage.*, vol. 223, pp. 1–17, Nov. 2020.
[2] X. Zheng, G. Chen, W. Cao, H. Xu, R. Zhao, Q. Xu, M. Kramer, D. L. Touzé, A. G. L. Borthwick, and Y. Li, "On the energy conversion characteristics of a top-mounted pitching absorber by using smoothed particle hydrodynamics," *Energy Convers. Manage.*, vol. 250, Dec. 2021, Art. no. 114893.
[3] Y. Li and Y.-H. Yu, "A synthesis of numerical methods for modeling wave energy converter-point absorbers," *Renew. Sustain. Energy Rev.*, vol. 16, no. 6, pp. 4352–4364, Aug. 2012.
[4] L. Zhu, T. Tian, J. Jiang, W. Wu, K. Lu, and C.-S. Koh, "A novel single-helix magnetic lead screw for wave energy converter," in *Proc. IECON 46th Annu. Conf. IEEE Ind. Electron. Soc.*, Oct. 2020, pp. 2807–2812.
[5] D. Valério, P. Beirão, and J. Sá da Costa, "Optimisation of wave energy extraction with the archimedes wave swing," *Ocean Eng.*, vol. 34, nos. 17–18, pp. 2330–2344, Dec. 2007.
[6] J. V. Ringwood, G. Bacelli, and F. Fusco, "Energy-maximizing control of wave-energy converters: The development of control system technology to optimize their operation," *IEEE Control Syst.*, vol. 34, no. 5, pp. 30–55, Oct. 2014.
[7] L. Huang, M. Hu, H. Yu, C. Liu, and Z. Chen, "Design and experiment of a direct-drive wave energy converter using outer-PM linear tubular generator," *IET Renew. Power Gener.*, vol. 11, no. 3, pp. 353–360, Feb. 2017.
[8] W. Sheng and A. Lewis, "Power takeoff optimization for maximizing energy conversion of wave-activated bodies," *IEEE J. Ocean. Eng.*, vol. 41, no. 3, pp. 529–540, Jul. 2016.
[9] E. Tedeschi, M. Carraro, M. Molinas, and P. Mattavelli, "Effect of control strategies and power take-off efficiency on the power capture from sea waves," *IEEE Trans. Energy Convers.*, vol. 26, no. 4, pp. 1088–1098, Dec. 2011.
[10] J. Falnes, *Ocean Waves and Oscillating Systems: Linear Interactions Including Wave-Energy Extraction*. Cambridge, U.K.: Cambridge Univ. Press, 2002, pp. 51–54.
[11] K. Budal and J. Falnes, "Interacting point absorbers with controlled motion," in *Power From Sea Waves*, B. M. Count, Ed. New York, NY, USA: Academic, 1980.
[12] Z. Feng and E. C. Kerrigan, "Latching declutching control of wave energy converters using derivative-free optimization," *IEEE Trans. Sustain. Energy*, vol. 6, no. 3, pp. 773–780, Jul. 2015.
[13] W. Huang and J. Yang, "A novel piecewise velocity control method using passivity-based controller for wave energy conversion," *IEEE Access*, vol. 8, pp. 59029–59043, 2020.
[14] F. Fusco and J. V. Ringwood, "A simple and effective real-time controller for wave energy converters," *IEEE Trans. Sustain. Energy*, vol. 4, no. 1, pp. 21–30, Jan. 2013.
[15] J. A. Cretel, A. W. Lewis, G. P. Thomas, and G. Lightbody, "A critical assessment of latching as a control strategy for wave-energy point absorbers," in *Proc. 31st Int. Offshore Polar Eng. Conf.*, Maui, HI, USA, 2011, pp. 680-686.
[16] X. Xiao, X. Huang, and Q. Kang, "A hill-climbing-method-based maximum-power-point-tracking strategy for direct-drive wave energy converters," *IEEE Trans. Ind. Electron.*, vol. 63, no. 1, pp. 257–267, Jan. 2016.
[17] Q. Sun, J. Wan, and S. Liu, "Estimation of sea level variability in the China sea and its vicinity using the SARIMA and LSTM models," *IEEE J. Sel. Topics Appl. Earth Observ. Remote Sens.*, vol. 13, pp. 3317–3326, 2020.
[18] (2010). *DNV, Environmental Conditions and Environmental Loads*. Accessed: Mar. 2017. [Online] Alable: ttps://rules.dnvgl.com/docs/pdf/DNV/codes/docs/2010-10/RP-C205.pdf
[19] W. Yang, Y. Liang, J. Leng, and M. Li, "The autocorrelation function obtained from the pierson-moskowitz spectrum," in *Proc. Global Oceans, Singapore U.S. Gulf Coast*, Oct. 2020, pp. 1–4.
[20] J. Prendergast, M. Li, and W. Sheng, "A study on the effects of wave spectra on wave energy conversions," *IEEE J. Ocean. Eng.*, vol. 45, no. 1, pp. 271–283, Jan. 2020.
[21] L. Li, Z. Yuan, Y. Gao, and X. Zhang, "Wave force prediction effect on the energy absorption of a wave energy converter with real-time control," *IEEE Trans. Sustain. Energy*, vol. 10, no. 2, pp. 615–624, Apr. 2019.
[22] P. Tokat and T. Thiringer, "Sizing of IPM generator for a single point absorber type wave energy converter," *IEEE Trans. Energy Convers.*, vol. 33, no. 1, pp. 10–19, Mar. 2018.
[23] J. S. Park, B.-G. Gu, J. R. Kim, I. H. Cho, I. Jeong, and J. Lee, "Active phase control for maximum power point tracking of a linear wave generator," *IEEE Trans. Power Electron.*, vol. 32, no. 10, pp. 7651–7662, Oct. 2017.
[24] R. K. Holm, N. I. Berg, M. Walkusch, P. O. Rasmussen, and R. H. Hansen, "Design of a magnetic lead screw for wave energy conversion," *IEEE Trans. Ind. Appl.*, vol. 49, no. 6, pp. 2699–2708, Nov. 2013.
[25] J. Falnes, *Ocean Waves and Oscillating Systems: Linear Interactions Including Wave-Energy Extraction*. Cambridge, U.K.: Cambridge Univ. Press, 2002, pp. 4–10.
[26] E. Tedeschi and M. Molinas, "Tunable control strategy for wave energy converters with limited power takeoff rating," *IEEE Trans. Ind. Electron.*, vol. 59, no. 10, pp. 3838–3846, Oct. 2012.
[27] S. Mirjalili, S. M. Mirjalili, and A. Lewis, "Grey wolf optimizer," *Adv. Eng. Softw.*, vol. 69, pp. 46–61, Mar. 2014.

LIXUN ZHU was born in Baotou, China. He received the Ph.D. degree in electrical engineering from Chungbuk National University, South Korea, in 2018.

He is currently a Lecturer with the Department of Logistics Engineering, Shanghai Maritime University, China. His research interests include renewable energy systems, motor design, and hysteresis modeling. His research has been supported by the National Natural Science Foundation of China, and Shanghai Sailing Program.

ZHAOYANG YAO was born in Shangqiu, China, in 1995. He received the B.S. degree in electrical engineering from the Luoyang Institute of Science and Technology. He is currently pursuing the master's degree with the Department of Logistics Engineering, Shanghai Maritime University, China.

His research interest includes renewable energy systems.

WEI LI (Member, IEEE) was born in Suihua, China. She received the B.S. and M.S. degrees in electrical engineering from the Harbin Institute of Technology, Harbin, China, in 2005 and 2007, respectively, and the Ph.D. degree in electrical engineering from Chungbuk National University, Chungbuk, South Korea, in 2011.

She has been an Assistant Professor with the School of Electronics and Information Engineering, Tongji University, Shanghai, China, since 2012, where she is currently an Associate Professor. Her current research interests include hysteresis modeling, finite element method, partial element equivalent method and their applications, and control of electrical machines.